Monthly Notices of the ROYAL ASTRONOMICAL SOCIETY

MNRAS **511,** 457–471 (2022) https://doi.org/10.1093/mnras/stac033
Advance Access publication 2022 January 12

Binary companions triggering fragmentation in self-gravitating discs

James Cadman,[1,2]★ Cassandra Hall [3,4] Clémence Fontanive [5] and Ken Rice [1,2]

[1]*SUPA, Institute for Astronomy, University of Edinburgh, Blackford Hill, Edinburgh EH9 3HJ, UK*
[2]*Centre for Exoplanet Science, University of Edinburgh, Edinburgh EH9 3HJ, UK*
[3]*Department of Physics and Astronomy, The University of Georgia, Athens, GA 30602, USA*
[4]*Center for Simulational Physics, The University of Georgia, Athens, GA 30602, USA*
[5]*Center for Space and Habitability, University of Bern, CH-3012 Bern, Switzerland*

Accepted 2021 December 30. Received 2021 December 8; in original form 2021 October 12

ABSTRACT

Observations of systems hosting close-in (<1 au) giant planets and brown dwarfs ($M \gtrsim 7\,M_{Jup}$) find an excess of binary-star companions, indicating that stellar multiplicity may play an important role in their formation. There is now increasing evidence that some of these objects may have formed via fragmentation in gravitationally unstable discs. We present a suite of 3D smoothed particle hydrodynamics simulations of binary-star systems with circumprimary self-gravitating discs, which include a realistic approximation to radiation transport, and extensively explore the companion's orbital parameter space for configurations that may trigger fragmentation. We identify a 'sweet spot' where intermediate separation binary companions ($100\,\text{au} \lesssim a \lesssim 400\,\text{au}$) can cause a marginally stable disc to fragment. The exact range of ideal binary separations is a function of the companion's eccentricity, inclination, and mass. Heating is balanced by efficient cooling, and fragmentation occurs inside a spiral mode driven by the companion. Short separation, disc-penetrating binary encounters ($a \lesssim 100\,\text{au}$) are prohibitive to fragmentation, as mass stripping and disc heating quench any instability. This is also true of binary companions with high orbital eccentricities ($e \gtrsim 0.75$). Wide separation companions ($a \gtrsim 500\,\text{au}$) have little effect on the disc properties for the set-up parameters considered here. The sweet spot found is consistent with the range of binary separations that display an excess of close-in giant planets and brown dwarfs. Hence, we suggest that fragmentation triggered by a binary companion may contribute to the formation of these substellar objects.

Key words: accretion, accretion discs – gravitation – instabilities – planets and satellites: formation – stars: formation.

1 INTRODUCTION

There are both theoretical (Lin & Pringle 1987; Rice, Mayo & Armitage 2010) and observational (Rodríguez et al. 2005; Tobin et al. 2012, 2015) indications that during the earliest stages of star formation, protostellar disc masses may be a significant fraction of the mass of the central protostar. If so, these discs would be susceptible to the growth of a gravitational instability (GI; Toomre 1964).

The evolution of a gravitationally unstable disc can follow two basic pathways. It can settle into a quasi-steady state (Paczynski 1978) in which spiral density waves act to drive angular momentum outwards, allowing mass to accrete on to the central protostar (Lin & Pringle 1987; Laughlin & Bodenheimer 1994; Lodato & Rice 2004). Recent observations of very young protostellar systems have shown the presence of spirals (Pérez et al. 2016), consistent with the disc being gravitationally unstable (Dong et al. 2015; Hall et al. 2016, 2018, 2020; Meru et al. 2017; Cadman et al. 2020b; Paneque-Carreño et al. 2021; Veronesi et al. 2021).

The other potential pathway is that the GI can lead to a disc becoming so unstable that it fragments into bound objects that could then contract to become gas giant planets, or brown dwarfs (Boss 1997, 2000; Mayer et al. 2002; Durisen et al. 2007). This outcome, however, requires not only that the disc is gravitationally unstable, but also that it can also cool very efficiently (Gammie 2001; Rice et al. 2003). Such conditions are unlikely to be satisfied in the inner parts of protostellar discs (Rafikov 2005; Clarke 2009; Rice & Armitage 2009), suggesting that this pathway is unlikely to play a dominant role in the *in situ* formation of the known close-in gas giant planets/exoplanets (Boley 2009; Johnson & Li 2013).

However, it is possible that such a process may operate in the outer parts of extended protostellar discs (Stamatellos & Whitworth 2009; Vorobyov & Basu 2010), potentially explaining the origin of some directly imaged, wide-orbit planetary-mass and brown dwarf companions (Nero & Bjorkman 2009; Kratter, Murray-Clay & Youdin 2010; Cadman, Rice & Hall 2021; Humphries et al. 2021). It has been shown that fragmentation is favoured in discs around higher mass stars (Cadman et al. 2020a; Haworth et al. 2020), consistent with results from direct-imaging surveys that find an excess of wide-orbit giant planets in these systems (Nielsen et al. 2019). Population synthesis models (Forgan & Rice 2013; Forgan et al. 2018) suggest that the mass distribution of planets formed via GI is indeed consistent with results from direct-imaging surveys of wide-orbit giant planets and brown dwarfs (Vigan et al. 2017, 2021).

It has also been suggested that objects that form via GI on wide orbits could migrate inwards rapidly (Baruteau, Meru & Paardekooper 2011) and potentially undergo tidal stripping (Boley et al. 2010;

★ E-mail: cadman@roe.ac.uk

Nayakshin 2010) to produce close-in planets with a wide range of masses (Nayakshin & Fletcher 2015). However, hydrodynamics simulations of such systems show that these objects either stay on wide orbits or are destroyed during the migration process (Hall, Forgan & Rice 2017). Population synthesis models also suggest that such an outcome is relatively rare, and that most objects that form via GI will remain on wide orbits as giant planets, or brown dwarfs (Forgan & Rice 2013; Forgan et al. 2018). Such objects could, though, still be scattered on to highly eccentric orbits that can then tidally circularize on to close-in orbits (Rice et al. 2015). This will tend to form gas giant planets, or brown dwarfs, with very close-in circular orbits (with orbital properties similar to those of 'hot' Jupiters) or eccentric orbits that are still undergoing tidal circularization.

Given that the scatterer is likely to be a companion to the host star, this motivated a search for companions to systems with close-in massive planets, or brown dwarfs (Fontanive et al. 2019). The results of this search did indeed indicate a binary fraction twice as high as for field stars on projected separations between 20 and 10 000 au. However, only about half of these systems were consistent with high-eccentricity migration through secular interactions with the outer stellar companion, the others being on orbits where the tidal circularization time-scale was far too long to explain their origin (Fontanive et al. 2019).

None the less, even if the close-in objects were not scattered on to their current orbits, the high binary fraction for these systems suggests that the existence of a companion may still influence their formation. There are also indications that some of these objects may have formed via GI. The sample of stars studied in Fontanive et al. (2019), hosting close-in companions with masses between 7 and 60 M_{Jup}, has a mean metallicity of $\langle[Fe/H]\rangle = -0.12$, consistent with the mean field metallicity (Moe, Kratter & Badenes 2019). This is substantially lower than the mean metallicity for hosts to genuine hot Jupiters (0.2–4 M_{Jup}) of $\langle[Fe/H]\rangle = 0.23$ (Santos, Israelian & Mayor 2004; Fischer & Valenti 2005), which also do not show the same excess in multiplicity frequency (Ngo et al. 2016; Moe & Kratter 2019).

This lower mass planetary population is thought to have formed via the alternative scenario for planet formation, core accretion (CA; Pollack et al. 1996). This formation mechanism shows a strong metallicity dependence in the formation of giant planets with masses above a few Jupiter masses (Mordasini et al. 2012; Jenkins et al. 2017). In contrast, the GI formation process has no metallicity dependence (Meru & Bate 2010), and preferentially forms massive planets or brown dwarfs (Kratter et al. 2010; Forgan & Rice 2011), with a transition at around ∼4–10 M_{Jup} between the two mechanisms (Schlaufman 2018).

This suggests that only the most massive planetary and brown dwarf companions, likely forming via GI, are affected by stellar binarity. Fontanive & Bardalez Gagliuffi (2021) recently confirmed this idea, finding that close-in exoplanets and substellar companions with masses of several Jupiter masses and above are almost exclusively observed in binary-star systems with separations of a few hundred au or less. In contrast, sub-Jovian and wide giant planets are less frequently seen in multiple-star systems, mostly observed in binaries with wider separations, and show similar planet properties when compared to the population of planets orbiting single and binary stars (Fontanive & Bardalez Gagliuffi 2021). We therefore investigate how the presence of a companion at a few hundred au can influence the likelihood of a disc undergoing fragmentation and forming such high-mass planetary systems.

There is little agreement in the literature as to whether binary companions or stellar flyby events can trigger fragmentation in a disc that would be marginally stable in isolation. Early work considering isothermal discs suggested that encounters during a flyby event could trigger fragmentation (Boffin et al. 1998; Watkins et al. 1998a,b). Boss (2006) also found that a binary star will act to promote fragmentation, as the spiral arms driven by the companion will typically go on to form self-gravitating clumps. Other authors, however, found that tidal heating during the binary orbit generally acts to stabilize the disc against fragmentation (Nelson 2000; Mayer et al. 2005; Lodato et al. 2007; Forgan & Rice 2009). While none of their simulations resulted in fragmentation, and the majority of their results suggest that the effect of encounters is to prohibit fragmentation, Forgan & Rice (2009) find that, for some orbital parameters, their discs become more unstable over a larger range of radii, suggesting that there may be some region of parameter space that is favourable to fragmentation. It has also been shown that once a fragment forms in a GI disc, further fragmentation may be triggered as material is channelled inwards causing the inner spirals to become sufficiently dense to fragment (Meru 2015).

In this paper, we present a suite of smoothed particle hydrodynamics (SPH) simulations of binary-star systems. We extensively test the parameter space of binary orbital properties for configurations that may trigger fragmentation in discs that would be marginally stable in isolation. We evolve a total of 62 discs, which, to the authors' knowledge, represents the most thorough search of this parameter space to date, and in each simulation we model realistic cooling through the Forgan et al. (2009) hybrid radiative transfer method. Section 2 details the various disc set-ups explored in our simulations. Section 3 presents the results obtained, which we discuss in Section 4. Our conclusions are presented in Section 5.

2 METHODS – SPH SIMULATIONS

We simulate a three-dimensional gaseous disc using SPH, a Lagrangian method where a continuous fluid is discretized as N pseudo-particles (Benz 1990; Monaghan 1992). We employ the PHANTOM SPH code (Price et al. 2018), which has been modified to include the radiative transfer method introduced in Forgan et al. (2009); a hybrid cooling approach that combines the polytropic cooling approximation from Stamatellos et al. (2007) and flux-limited diffusion (e.g. Mayer et al. 2007b). We also include the standard SPH artificial viscosity, with parameters $\alpha_{SPH} = 0.1$ and $\beta_{SPH} = 0.2$.

Each disc is initialized with $N = 1 \times 10^6$ SPH particles, distributed such that the initial surface density profile of the disc is $\Sigma(R) = \Sigma_0(R/R_0)^{-1.5}$ and the temperature profile is $T(R) = T_0(R/R_0)^{-1.0}$ between $R_0 = 1$ au and $R_{out} = 100$ au. In each disc, T_0 and Σ_0 are determined self-consistently, with $T_0 = 374$ K for all discs set up here, and Σ_0 varying with the disc mass being considered. Any particles that fall within R_0 are accreted on to the central star, which is represented as a point mass particle. When considering binary-star systems, we set up circumprimary discs only, and the companion star behaves as a gravitationally bound point mass, modelled using a sink particle.

2.1 Suite of SPH models

To effectively explore the parameter space in binary-star separation, a, orbital eccentricity, e, orbital inclination, i, and companion star mass, $M_{*,companion}$, we set up four suites of discs – one for studying each variable individually. In each case, the disc set-up parameters are selected to be close to where we find the limit for disc fragmentation

Table 1. SPH disc set-up parameters for the reference run of discs with no companion star. Final states of these discs are shown in Fig. 1.

$N_{\rm SPH}$	$R_{\rm out,disc}$	M_*	$M_{\rm disc}$
1×10^6	100 au	$1\,{\rm M}_\odot$	$[0.1, 0.2, 0.3, 0.4]\,{\rm M}_\odot$

to be, identified during our reference run of discs that are detailed below.

2.1.1 *Reference run of discs with no companion*

We initially set up a reference run of discs with no companion. This allows us to understand how our discs would evolve in isolation, while also being able to identify the region of parameter space where our discs are near to the limit for fragmentation. We set up four discs here with masses $M_{\rm disc} = 0.1$, 0.2, 0.3, and $0.4\,{\rm M}_\odot$, and a parent star of mass $M_* = 1.0\,{\rm M}_\odot$. The value of Σ_0 for each of these discs, and all subsequent discs of the same mass, are 322, 644, 966, $1288\,{\rm g\,cm^{-2}}$, respectively. A summary of these set-up parameters can be found in Table 1.

2.1.2 *Varying binary-star separation*

In the first of our suites that include a companion star, we aim to determine how binary separation affects a disc's susceptibility to fragmentation. We set up a grid of 16 systems in which we vary a between 100 and 1000 au and $M_{\rm disc}$ between 0.1 and $0.4\,{\rm M}_\odot$, as for the reference runs. We then explore four additional cases of a with finer steps in binary separation between $a = 150$–400 au and a fixed disc mass $M_{\rm disc} = 0.2\,{\rm M}_\odot$. In all the set-ups, we consider a primary star with mass $M_{*,\rm primary} = 1.0\,{\rm M}_\odot$ and a companion star with mass $M_{*,\rm companion} = 0.2\,{\rm M}_\odot$, hence a stellar mass ratio $q_{\rm binary} = 0.2$. For this initial suite, we set up binaries on circular orbits in the plane of the disc, with $e = 0$ and $i = 0$. These disc set-ups are summarized in Tables 2 and 3.

Results from this initial suite of discs, where we vary the companion's semimajor axis, were then used to inform the range of semimajor axes considered for the subsequent suites of disc simulations.

2.1.3 *Varying orbital eccentricity*

We then wish to study the effect of varying the orbital eccentricity of the binary orbit. 18 new discs are set-up where we introduce eccentricities, $e = 0.25$, 0.5, and 0.75. We vary the binary separation between $a = 150$–500 au while keeping the disc mass constant at $M_{\rm disc} = 0.2\,{\rm M}_\odot$. In all cases, we consider a primary star mass, $M_{*,\rm primary} = 1.0\,{\rm M}_\odot$, a companion star mass, $M_{*,\rm companion} = 0.2\,{\rm M}_\odot$, and binary orbits in the plane of the disc, with $i = 0$. A summary of these disc set-ups is outlined in Table 4.

2.1.4 *Varying orbital inclination*

A third suite of discs is set up where we study the effect of varying the companion star's orbital inclination relative to the plane of the disc. We set up 12 new discs that include inclinations $i = 30°$, 60°, and 90°. We consider binary separations in the range $a = 100$–250 au, while keeping the disc mass constant at $M_{\rm disc} = 0.2\,{\rm M}_\odot$. In each case, we consider a primary star mass, $M_{*,\rm primary} = 1.0\,{\rm M}_\odot$, a companion star mass, $M_{*,\rm companion} = 0.2\,{\rm M}_\odot$, and circular binary orbits with $e = 0$. A summary of these disc set-ups is outlined in Table 5.

2.1.5 *Varying companion star mass*

Finally, we set up a suite of discs to explore the effect of varying the mass of the companion star. We set up a grid of discs that includes eight new set-ups, where we introduce companion star masses $M_{*,\rm companion} = 0.1$ and $0.5\,{\rm M}_\odot$. We vary the binary separation between $a = 150$–400 au, while keeping the disc mass constant at $M_{\rm disc} = 0.2\,{\rm M}_\odot$. For all disc set-ups, we consider a primary star mass, $M_{*,\rm primary} = 1.0\,{\rm M}_\odot$, and circular binary orbits in the plane of the disc, with $e = 0$ and $i = 0$. A summary of these disc set-ups is outlined in Table 6.

3 RESULTS

Results from the final states of all the discs simulated here are summarized in Table 7. In all cases, we allow the discs to evolve for at least 5 orbital periods at the disc outer edge ($R_{\rm out} = 100$ au), equivalent to $t = 5000$ yr, or until fragmentation occurs. In the case of the wide-orbit binary systems, for which the binary orbit is longer than 5 orbital periods at $R_{\rm out} = 100$ au, we allow the simulations to evolve for at least a full binary orbit. We define a simulation as having fragmented when a local clump forms where the density is significantly higher than the surrounding disc gas. Typically, these clumps have densities that are a few orders of magnitude greater than the surrounding gas.

3.1 Reference run of discs with no companion

Fig. 1 shows the final states of the reference run of discs with no companion star included. Set-up parameters for these discs are outlined in Section 2.1.1 and summarized in Table 1. We find the lower mass limit for disc fragmentation to be in the range $0.2 < M_{\rm disc} < 0.3\,{\rm M}_\odot$. The disc with $M_{\rm disc.} = 0.2\,{\rm M}_\odot$ is able to evolve for the full simulation time without fragmenting, while the disc with $M_{\rm disc} = 0.3\,{\rm M}_\odot$ fragments quickly, after 700 yr of evolution.

In Fig. 3, we plot the azimuthally averaged mid-plane disc properties from some of the systems simulated here. We include plots of the Toomre parameter, Q, where (Toomre 1964)

$$Q = \frac{c_{\rm s}\Omega}{\pi {\rm G}\Sigma}. \tag{1}$$

A disc will become susceptible to fragmentation when $Q \lesssim 1$. We also plot the disc cooling time, $t_{\rm cool} (= u/\dot{u})$, from Forgan et al. (2009), and the dimensionless cooling parameter, $\beta_{\rm cool} = t_{\rm cool}\Omega$, where $\Omega = \sqrt{{\rm G}M_*/r^3}$ is the Keplerian frequency at a given radius. The term $\beta_{\rm cool}$ quantifies how the disc cooling time compares to the dynamical time. Early work has shown that fragmentation may occur if the disc is able to cool on dynamical time-scales, with $\beta_{\rm cool} \lesssim 3$ (Gammie 2001; Rice et al. 2003).

From Fig. 3, we find that the system with $M_{\rm disc} = 0.2\,{\rm M}_\odot$ reaches a marginally stable final state with $Q_{\rm min} = 1.06$ at $R = 74$ au, and $\beta_{\rm cool,\,min} = 9.75$ at $R = 100$ au.

In order to ensure that the fragmentation threshold found here is independent of the discs' initial set-ups, we also ran each disc such that $Q \approx 1$ at $R = R_{\rm out}$, by adjusting the value of the disc aspect ratio (H/R) at $R = R_{\rm out}$. Again, we found the limit for fragmentation to be in the range $0.2 < M_{\rm disc} < 0.3\,{\rm M}_\odot$.

Table 2. SPH disc set-up parameters for the initial suite of discs, where we explore the parameter space in binary semimajor axis and disc mass. Final states of these discs are shown in Fig. 2.

$N_{\rm SPH}$	$R_{\rm out,disc}$	$M_{*,\rm primary}$	$M_{*,\rm companion}$	a	$M_{\rm disc}$	e	i
1×10^6	100 au	$1\,{\rm M}_\odot$	$0.2\,{\rm M}_\odot$	[100, 250, 500, 1000] au	[0.1, 0.2, 0.3, 0.4] $\rm M_\odot$	0	0°

Table 3. SPH disc set-up parameters where we probe the parameter space in binary semimajor axis further, considering small changes in binary semimajor axis and keeping the disc mass constant. Final states of these discs are shown in Fig. 4.

$N_{\rm SPH}$	$R_{\rm out,disc}$	$M_{*,\rm primary}$	$M_{*,\rm companion}$	a	$M_{\rm disc}$	e	i
1×10^6	100 au	$1\,{\rm M}_\odot$	$0.2\,{\rm M}_\odot$	[150, 200, 325, 400] au	$0.2\,{\rm M}_\odot$	0	0°

Table 4. SPH disc set-up parameters where we explore the parameter space in binary semimajor axis and orbital eccentricity. Final states of these discs are shown in Fig. 5.

$N_{\rm SPH}$	$R_{\rm out,disc}$	$M_{*,\rm primary}$	$M_{*,\rm companion}$	a	$M_{\rm disc}$	e	i
1×10^6	100 au	$1\,{\rm M}_\odot$	$0.2\,{\rm M}_\odot$	[150, 200, 250, 325, 400, 500] au	$0.2\,{\rm M}_\odot$	[0.25,0.5,0.75]	0°

Table 5. SPH disc set-up parameters where we explore the parameter space in binary semimajor axis and binary inclination. Final states of these discs are shown in Fig. 6.

$N_{\rm SPH}$	$R_{\rm out,disc}$	$M_{*,\rm primary}$	$M_{*,\rm companion}$	a	$M_{\rm disc}$	e	i
1×10^6	100 au	$1\,{\rm M}_\odot$	$0.2\,{\rm M}_\odot$	[100, 150, 200, 250] au	$0.2\,{\rm M}_\odot$	0	[30°, 60°, 90°]

Table 6. Additional SPH disc set-up parameters where we explore the parameter space in binary semimajor axis and companion mass. Final states of these discs are shown in Fig. 7.

$N_{\rm SPH}$	$R_{\rm out,disc}$	$M_{*,\rm primary}$	$M_{*,\rm companion}$	a	$M_{\rm disc}$	e	i
1×10^6	100 au	$1\,{\rm M}_\odot$	[0.1,0.5] $\rm M_\odot$	[150, 250, 325, 400] au	$0.2\,{\rm M}_\odot$	0	0°

3.2 Varying binary separation

3.2.1 Initial suite of discs

Results from the initial suite of discs where we vary binary separation and disc mass are displayed in Fig. 2. Set-up parameters for these discs are outlined in Section 2.1.2 and summarized in Table 2. As with the results in Section 3.1, we also ran each of these discs with slightly different initial Q-profiles to ensure our conclusions remain consistent.

When comparing the results in Fig. 2 to those from the reference run in Fig. 1, we find one disc configuration, with $M_{\rm disc} = 0.2\,{\rm M}_\odot$ and $a = 250$ au, where the simulation results in fragmentation, and its analogue from the reference run, with $M_{\rm disc} = 0.2\,{\rm M}_\odot$ and no companion star, did not. The companion star's initial eccentricity is $e = 0$; however, energy exchange with disc material throughout the companion's orbit results in a periastron binary separation of $r_{\rm peri,actual} = 186$ au. As the companion approaches and passes through periastron, an $m = 2$ spiral mode propagates through the disc generating a bump in the surface density at $R \approx 60$ au.

Comparing the disc properties in Fig. 3 for the system where $a = 250$ au and $M_{\rm disc} = 0.2\,{\rm M}_\odot$ immediately before fragmentation occurs (at $t \approx 2700$ yr), and the properties from the final state of the analogue disc from the reference run (where $M_{\rm disc} = 0.2\,{\rm M}_\odot$), we observe how the surface density increases in the disc of the $a = 250$ au system, consistent with the location of the spirals driven by the companion. Efficient cooling, evident from the drop in $t_{\rm cool}$ between ≈ 60 and 90 au, is able to prevent the disc temperature from increasing significantly at the spiral location. Hence, Q can drop to below $Q = 1$ and fragmentation ensues. For the system where $a = 250$ au, immediately before the disc fragments, we find $\beta_{\rm cool,min} = 2.92$ at $R = 75$ au.

Binaries on wide orbits ($a = 500$, 1000 au) converge to the single-star solution, where the mass limit for fragmentation is $0.2\,{\rm M}_\odot < M_{\rm disc} < 0.3\,{\rm M}_\odot$. In Fig. 3, we also plot the azimuthally averaged mid-plane disc properties for the set-up where $M_{\rm disc} = 0.2\,{\rm M}_\odot$ and $a = 500$ au at the time of periastron passage. The temperature profile and Q-profile are almost identical to the analogue disc from the reference run, with $Q_{\rm min} = 1.05$ at $R = 75$ au. Similarly, we find no significant bump in the surface density profile that would be consistent with a spiral being driven by the companion star. The $M_{\rm disc} = 0.3\,{\rm M}_\odot$ system with a companion at $a = 500$ au fragments quickly, as it did around a single star.

Binaries with small semimajor axes, whose orbits result in the companion star passing through the disc ($a = 100$ au), are found to be prohibitive to fragmentation. In Fig. 3, we plot the azimuthally averaged mid-plane properties for the disc with $a = 100$ au and $M_{\rm disc} = 0.2\,{\rm M}_\odot$, at the point of periastron passage (where $r_{\rm peri,actual} = 78$ au). As the companion moves through the disc the mid-plane temperature increases, while material is simultaneously ejected from the outer disc and channelled towards the inner disc. The final surface density profiles for the $a = 100$ au discs, set up with $M_{\rm disc} = 0.1$ and $0.2\,{\rm M}_\odot$, are consequently truncated at $a \approx 40$ au, with final disc masses $M_{\rm disc} = 0.06$ and $0.12\,{\rm M}_\odot$, respectively. Hence, no fragmentation can occur. The massive discs with $M_{\rm disc} \geq 0.3\,{\rm M}_\odot$ are still able to fragment quickly, before completing a full binary orbital period, in a spiral arm that trails the path of the companion star.

Table 7. Summary of all discs simulated here, and whether they did or did not fragment. Black ticks: Disc fragmented and so did its reference run analogue. Double green ticks: Disc fragmented when the reference run analogue did not. Black crosses: Did not fragment. $r_{\rm peri,actual}$ = NR ('not reached') denotes systems where the simulation ended before reaching $r_{\rm peri,actual}$, as the disc had already fragmented.

	a	$M_{\rm disc}$	$M_{*,\rm primary}$	$M_{*,\rm companion}$	e	i	$r_{\rm peri,calc}$	$r_{\rm peri,actual}$	Fragmented?	$t_{\rm frag}$
Reference runs:	–	0.1 $M_\odot$	1 $M_\odot$	–	–	–	–	–	✗	–
	–	0.2 $M_\odot$	1 $M_\odot$	–	–	–	–	–	✗	–
	–	0.3 $M_\odot$	1 $M_\odot$	–	–	–	–	–	✓	700 yr
	–	0.4 $M_\odot$	1 $M_\odot$	–	–	–	–	–	✓	500 yr
Varying binary separation:	100 au	0.1 $M_\odot$	1 $M_\odot$	0.2 $M_\odot$	0	0°	100 au	87 au	✗	–
	100 au	0.2 $M_\odot$	1 $M_\odot$	0.2 $M_\odot$	0	0°	100 au	78 au	✗	–
	100 au	0.3 $M_\odot$	1 $M_\odot$	0.2 $M_\odot$	0	0°	100 au	70 au	✓	600 yr
	100 au	0.4 $M_\odot$	1 $M_\odot$	0.2 $M_\odot$	0	0°	100 au	64 au	✓	500 yr
	250 au	0.1 $M_\odot$	1 $M_\odot$	0.2 $M_\odot$	0	0°	250 au	213 au	✗	–
	250 au	0.2 $M_\odot$	1 $M_\odot$	0.2 $M_\odot$	0	0°	250 au	186 au	✓✓	3050 yr
	250 au	0.3 $M_\odot$	1 $M_\odot$	0.2 $M_\odot$	0	0°	250 au	NR	✓	720 yr
	250 au	0.4 $M_\odot$	1 $M_\odot$	0.2 $M_\odot$	0	0°	250 au	NR	✓	540 yr
	500 au	0.1 $M_\odot$	1 $M_\odot$	0.2 $M_\odot$	0	0°	500 au	430 au	✗	–
	500 au	0.2 $M_\odot$	1 $M_\odot$	0.2 $M_\odot$	0	0°	500 au	373 au	✗	–
	500 au	0.3 $M_\odot$	1 $M_\odot$	0.2 $M_\odot$	0	0°	500 au	NR	✓	680 yr
	500 au	0.4 $M_\odot$	1 $M_\odot$	0.2 $M_\odot$	0	0°	500 au	NR	✓	445 yr
	1000 au	0.1 $M_\odot$	1 $M_\odot$	0.2 $M_\odot$	0	0°	1000 au	862 au	✗	–
	1000 au	0.2 $M_\odot$	1 $M_\odot$	0.2 $M_\odot$	0	0°	1000 au	758 au	✗	–
	1000 au	0.3 $M_\odot$	1 $M_\odot$	0.2 $M_\odot$	0	0°	1000 au	NR	✓	650 yr
	1000 au	0.4 $M_\odot$	1 $M_\odot$	0.2 $M_\odot$	0	0°	1000 au	NR	✓	500 yr
Additional separation runs:	150 au	0.2 $M_\odot$	1 $M_\odot$	0.2 $M_\odot$	0	0°	150 au	116 au	✓✓	750 yr
	200 au	0.2 $M_\odot$	1 $M_\odot$	0.2 $M_\odot$	0	0°	200 au	150 au	✓✓	1500 yr
	325 au	0.2 $M_\odot$	1 $M_\odot$	0.2 $M_\odot$	0	0°	325 au	240 au	✗	–
	400 au	0.2 $M_\odot$	1 $M_\odot$	0.2 $M_\odot$	0	0°	400 au	299 au	✗	–
Varying eccentricity:	150 au	0.2 $M_\odot$	1 $M_\odot$	0.2 $M_\odot$	0.25	0°	113 au	92 au	✓✓	900 yr
	150 au	0.2 $M_\odot$	1 $M_\odot$	0.2 $M_\odot$	0.5	0°	75 au	63 au	✗	–
	150 au	0.2 $M_\odot$	1 $M_\odot$	0.2 $M_\odot$	0.75	0°	38 au	39 au	✗	–
	200 au	0.2 $M_\odot$	1 $M_\odot$	0.2 $M_\odot$	0.25	0°	150 au	119 au	✓✓	1300 yr
	200 au	0.2 $M_\odot$	1 $M_\odot$	0.2 $M_\odot$	0.5	0°	100 au	81 au	✗	–
	200 au	0.2 $M_\odot$	1 $M_\odot$	0.2 $M_\odot$	0.75	0°	50 au	46 au	✗	–
	250 au	0.2 $M_\odot$	1 $M_\odot$	0.2 $M_\odot$	0.25	0°	188 au	147 au	✓✓	2000 yr
	250 au	0.2 $M_\odot$	1 $M_\odot$	0.2 $M_\odot$	0.5	0°	125 au	102 au	✓✓	1770 yr
	250 au	0.2 $M_\odot$	1 $M_\odot$	0.2 $M_\odot$	0.75	0°	63 au	54 au	✗	–
	325 au	0.2 $M_\odot$	1 $M_\odot$	0.2 $M_\odot$	0.25	0°	244 au	200 au	✗	–
	325 au	0.2 $M_\odot$	1 $M_\odot$	0.2 $M_\odot$	0.5	0°	163 au	134 au	✓✓	2750 yr
	325 au	0.2 $M_\odot$	1 $M_\odot$	0.2 $M_\odot$	0.75	0°	81 au	69 au	✗	–
	400 au	0.2 $M_\odot$	1 $M_\odot$	0.2 $M_\odot$	0.25	0°	300 au	236 au	✗	–
	400 au	0.2 $M_\odot$	1 $M_\odot$	0.2 $M_\odot$	0.5	0°	200 au	163 au	✓✓	3800 yr
	400 au	0.2 $M_\odot$	1 $M_\odot$	0.2 $M_\odot$	0.75	0°	100 au	84 au	✗	–
	500 au	0.2 $M_\odot$	1 $M_\odot$	0.2 $M_\odot$	0.25	0°	375 au	295 au	✗	–
	500 au	0.2 $M_\odot$	1 $M_\odot$	0.2 $M_\odot$	0.5	0°	250 au	204 au	✗	–
	500 au	0.2 $M_\odot$	1 $M_\odot$	0.2 $M_\odot$	0.75	0°	125 au	104 au	✗	–
Varying inclination:	100 au	0.2 $M_\odot$	1 $M_\odot$	0.2 $M_\odot$	0	30°	100 au	77 au	✗	–
	100 au	0.2 $M_\odot$	1 $M_\odot$	0.2 $M_\odot$	0	60°	100 au	74 au	✓✓	835 yr
	100 au	0.2 $M_\odot$	1 $M_\odot$	0.2 $M_\odot$	0	90°	100 au	75 au	✓✓	835 yr
	150 au	0.2 $M_\odot$	1 $M_\odot$	0.2 $M_\odot$	0	30°	150 au	114 au	✓✓	720 yr
	150 au	0.2 $M_\odot$	1 $M_\odot$	0.2 $M_\odot$	0	60°	150 au	115 au	✓✓	1045 yr
	150 au	0.2 $M_\odot$	1 $M_\odot$	0.2 $M_\odot$	0	90°	150 au	116 au	✓✓	1340 yr
	200 au	0.2 $M_\odot$	1 $M_\odot$	0.2 $M_\odot$	0	30°	200 au	151 au	✓✓	1600 yr
	200 au	0.2 $M_\odot$	1 $M_\odot$	0.2 $M_\odot$	0	60°	200 au	152 au	✓✓	2840 yr
	200 au	0.2 $M_\odot$	1 $M_\odot$	0.2 $M_\odot$	0	90°	200 au	153 au	✗	–
	250 au	0.2 $M_\odot$	1 $M_\odot$	0.2 $M_\odot$	0	30°	250 au	187 au	✗	–
	250 au	0.2 $M_\odot$	1 $M_\odot$	0.2 $M_\odot$	0	60°	250 au	189 au	✗	–
	250 au	0.2 $M_\odot$	1 $M_\odot$	0.2 $M_\odot$	0	90°	250 au	190 au	✗	–
Varying companion mass:	150 au	0.2 $M_\odot$	1 $M_\odot$	0.1 $M_\odot$	0	0°	150 au	110 au	✓✓	900 yr
	150 au	0.2 $M_\odot$	1 $M_\odot$	0.5 $M_\odot$	0	0°	150 au	112 au	✓✓	550 yr
	250 au	0.2 $M_\odot$	1 $M_\odot$	0.1 $M_\odot$	0	0°	250 au	181 au	✗	–
	250 au	0.2 $M_\odot$	1 $M_\odot$	0.5 $M_\odot$	0	0°	250 au	197 au	✓✓	1550 yr

Table 7 – *continued*

a	$M_{\rm disc}$	$M_{*,\rm primary}$	$M_{*,\rm companion}$	e	i	$r_{\rm peri,calc}$	$r_{\rm peri,actual}$	Fragmented?	$t_{\rm frag}$
325 au	0.2 $M_\odot$	1 $M_\odot$	0.1 $M_\odot$	0	0°	325 au	237au	✗	–
325 au	0.2 $M_\odot$	1 $M_\odot$	0.5 $M_\odot$	0	0°	325 au	256 au	✓✓	4000 yr
400 au	0.2 $M_\odot$	1 $M_\odot$	0.1 $M_\odot$	0	0°	400 au	292 au	✗	–
400 au	0.2 $M_\odot$	1 $M_\odot$	0.5 $M_\odot$	0	0°	400 au	315 au	✗	–

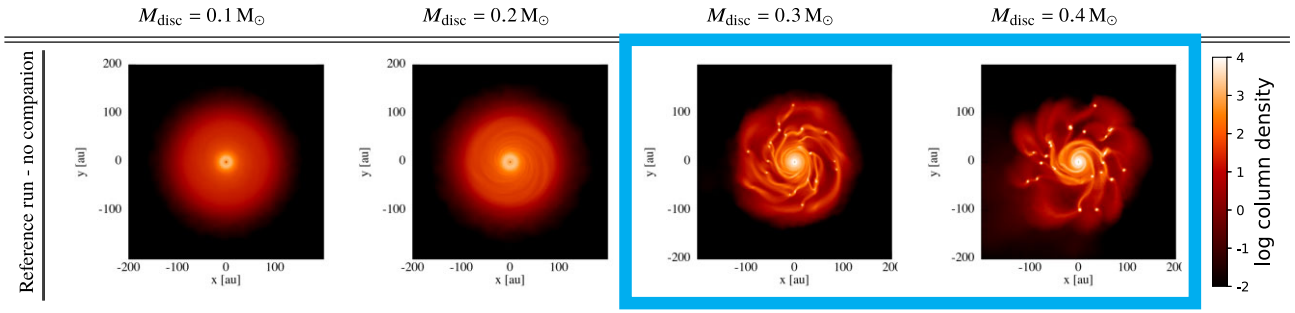

Figure 1. Final states of the reference run of disc set-ups with no companion star included. A summary of the disc set-up parameters laid out in Table 1, and outlined in detail in Section 2.1.1. Blue boxes are included to highlight the reference run discs that resulted in fragmentation.

3.2.2 Further probing the parameter space in binary separation

As the results in Fig. 2 indicate that there may be a sweet spot in binary separation at $a \approx 250$ au that can trigger fragmentation, we ran an additional set of discs where we probe this region of parameter space with greater granularity. This consists of four additional discs with $M_{\rm disc} = 0.2\,{\rm M}_\odot$ and $a = 150$, 200, 325, and 400 au. Set-up parameters for these are outlined in Section 2.1.2 and summarized in Table 3. Final states of these discs are shown in Fig. 4.

We find that the disc set-ups with binary semimajor axes between 150 au $\leq a \leq$ 250 au result in fragmentation. In the configuration with $a = 150$ au, the companion narrowly avoids passing through the outer extent of the disc, with $r_{\rm peri,actual} = 116$ au. As the companion approaches and passes through periastron, an $m = 2$ spiral mode propagates through the disc causing a significant drop in Q at the inner regions of one of these spirals, between 30 au $\leq R \leq$ 50 au, and four fragments initially form. All four of these fragments survive as the companion travels back towards apastron, as can be seen in the final state of the disc in Fig. 4. A similar process occurs in the system with $a = 200$ au.

As we increase the binary separation beyond $a = 250$ au the influence of the companion star becomes progressively weaker. Once $a \geq 325$ au the companion star can no longer trigger fragmentation in the disc. The spiral mode induced by the $a = 325$ au companion is much weaker than in the $a = 250$ au disc. We find that Q drops slightly in the outer disc of the $a = 325$ au system when compared to its analogue from the reference run (with $M_{\rm disc} = 0.2\,{\rm M}_\odot$ and no companion), but not enough to push the disc over the fragmentation threshold. Once we increase the binary semimajor axis to $a = 400$ au we find a similar result as with the $a = 500$ au system in the previous section. The surface density profile, Q-profile and temperature profile at periastron passage become increasingly similar to the final state of the reference run disc with $M_{\rm disc} = 0.2\,{\rm M}_\odot$.

3.3 Varying orbital eccentricity

So far we have only considered companion stars on circular orbits, with $e = 0$. In reality it is likely that there will be some orbital eccentricity. Hence, in this section, we simulate 18 new discs, introducing eccentricities, $e = 0.25$, 0.5, and 0.75. We consider set-up parameters found to be near to the limit for fragmentation, keeping the disc mass constant at $M_{\rm disc} = 0.2\,{\rm M}_\odot$, and varying a and e only. These set-ups are outlined in Section 2.1.3 and summarized in Table 4. Final states of these discs are shown in Fig. 5.

In the previous section, we found that companion stars with semimajor axes 150 au $\leq a \leq$ 250 au (116 au $\leq r_{\rm peri,actual} \leq$ 186 au) may induce fragmentation in a disc that would not fragment in isolation. When including eccentricity we find a wider range of semimajor axes are capable of inducing fragmentation, given that $r_{\rm peri,actual}$ falls roughly within the same range as found previously.

When including an eccentricity of $e = 0.5$ we find that disc set-ups with $a = 325$ au and $a = 400$ au now also result in fragmentation. The periastron distances observed in these simulations are $r_{\rm peri,actual} = 134$ au and $r_{\rm peri,actual} = 163$ au, respectively. Fragmentation occurs in a similar manner here to what was found in the previous section; an $m = 2$ spiral that is generated as the companion approaches and passes through periastron becomes unstable and forms bound, self-gravitating clumps.

We find that fragmentation occurs in this suite for a slightly lower $r_{\rm peri,actual}$ than was found in the previous section. In the configuration with $a = 150$ au and $e = 0.25$, corresponding to $r_{\rm peri,actual} = 92$ au, the companion passes through the very outer edge of the disc and a single fragment forms in the spiral 180° from the companion's location. Disc heating at periastron is much less here than was the case when $a = 100$ au and $e = 0$ ($r_{\rm peri,actual} = 78$ au), which was found to inhibit fragmentation. The amount of mass ejected is also significantly less here, with a final disc mass $M_{\rm disc} = 0.18\,{\rm M}_\odot$. What remains is a slightly more compact disc, truncated at $R \approx 75$ au.

For any companion that passes closer than $r_{\rm peri,actual} = 92$ au, the disc–star interaction becomes destructive. Disc material is dispersed as the companion passes through the disc, ejecting a significant amount of mass, leaving a compact, lower mass disc, thus entirely preventing fragmentation. All configurations here with $e = 0.75$ suffer this fate.

An interesting case is the disc set-up with $a = 500$ au and $e = 0.75$. Despite this system's actual periastron distance of $r_{\rm peri,actual} = 104$ au falling within the sweet spot found that may

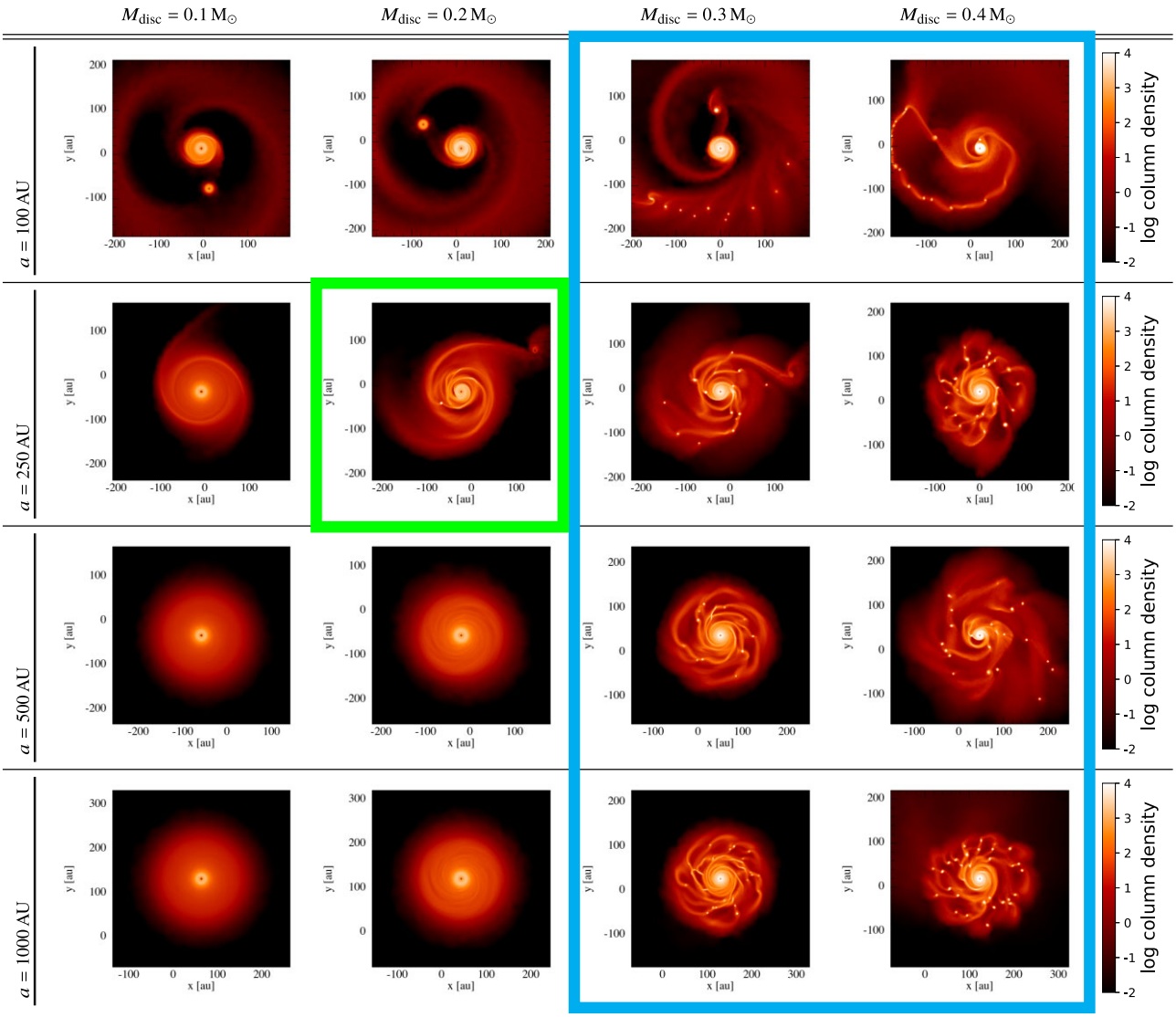

Figure 2. Final states of the discs where we vary the disc mass and the semimajor axis of the companion star. Disc set-up parameters are summarized in Table 2 and outlined in detail in Section 2.1.2. Blue boxes are included to highlight discs that resulted in fragmentation when their reference run analogues also fragmented. Green boxes are included to highlight disc configurations that resulted in fragmentation when their reference run analogue did not fragment.

induce fragmentation, no fragmentation occurs here. As the companion passes through periastron a self-gravitating clump begins to form at the inner edge of one of the spirals but immediately disperses as the companion quickly moves away from periastron. As the companion moves back towards apastron the disc stabilizes again.

3.4 Varying orbital inclination

In this section, we consider systems with some orbital inclination relative to the plane of the disc. We introduce inclinations $i = 30°$, 60°, and 90°, once again keeping the disc mass constant at $M_{\rm disc} = 0.2\,{\rm M}_\odot$ and varying the binary separation close to the limit for fragmentation. Disc set-up parameters are outlined in Section 2.1.4 and summarized in Table 5. Final states of these discs are shown in Fig. 6.

In the short orbit system, with $a = 100$ au, we find that including an inclination $i \geq 60°$ results in a less destructive disc–star interaction than when the companion orbits in the plane of the disc, hence fragmentation can occur. Despite their $r_{\rm peri,actual}$ being similar, the resulting surface density profile after the companion has passed through the plane of the disc is much less truncated when $i = 60°$ than was the case when $i = 0°$, extending to $R_{\rm out} \approx 80$ au after several binary orbital periods. An $m = 2$ spiral mode forms quickly, and a fragment forms at the inner edge of one the spirals, at $R = 55$ au. The fragment's orbit is initially slightly inclined relative to the disc, with $i \approx 8°$, but it quickly settles into the plane of the disc after an orbital period. The final state of the $i = 60°$ disc is more flared compared to when $i = 0°$, with $H/R = 0.15$ at $R = 100$ au compared to $H/R = 0.10$ at $R = 100$ au.

In the wider orbit systems, with $a = 200$ and 250 au, we find that including an inclination can weaken the disc–star interaction compared to when $i = 0°$ such that disc fragmentation no longer occurs. Considering the discs with $a = 250$ au, as we increase the companion's inclination from $i = 0°$ to $i = 90°$ we find that the $m = 2$ spiral mode generated by the companion becomes progressively less significant. When $i = 30°$, we observe a much smaller bump in the surface density profile when compared to the system with

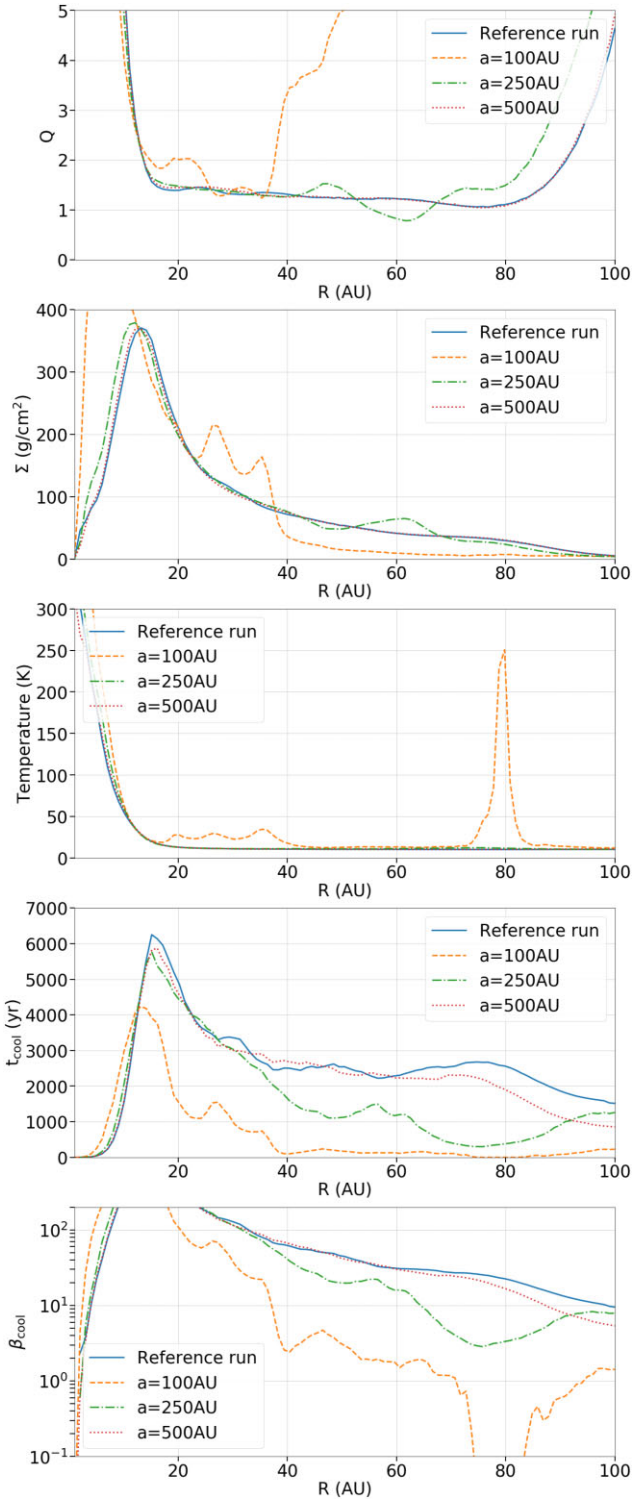

Figure 3. Azimuthally averaged mid-plane disc properties calculated from the $M_{\rm disc} = 0.2\,{\rm M}_{\odot}$ discs from the initial suite that includes a binary companion (set-up parameters in Table 2, final states in Fig. 2). We plot the reference run final state, the $a = 100$ au run at periastron, the $a = 250$ au run immediately before fragmentation, and the $a = 500$ au run at periastron.

$i = 0°$. Hence, the Q-profile remains relatively flat, and no fragmentation occurs. For the discs with $a = 200$ au, only a single fragment forms when $i = 60°$, and increasing the inclination to $i = 90°$ prevents fragmentation from happening altogether.

3.5 Varying companion mass

The gravitational influence of the companion star on the disc will vary with the star's mass. Hence, we set up eight new discs where we explore the parameter space in $M_{*,\rm companion}$ and a for configurations that result in fragmentation. In particular, we focus on how varying the companion star's mass affects the binary separations that are capable of inducing fragmentation.

Discs are set-up with parameters close to the fragmentation limit found until now, keeping the disc mass constant at $M_{\rm disc} = 0.2\,{\rm M}_{\odot}$ and varying $M_{*,\rm companion}$ and a only. We introduce new companion masses $M_{*,\rm companion} = 0.1\,{\rm M}_{\odot}$ and $M_{*,\rm companion} = 0.5\,{\rm M}_{\odot}$. These set-ups are outlined in Section 2.1.5 and summarized in Table 6. The final states of these discs are shown in Fig. 7.

Considering the discs with $a = 150$ au, we find that both of the new set-ups, with $M_{*,\rm companion} = 0.1\,{\rm M}_{\odot}$ and $M_{*,\rm companion} = 0.5\,{\rm M}_{\odot}$, result in fragmentation, with a trend for the discs to fragment faster with increasing $M_{*,\rm companion}$. We find $t_{\rm frag} = 900$, 750, and 550 yr when $M_{*,\rm companion} = 0.1$, 0.2, and $0.5\,{\rm M}_{\odot}$, respectively.

When $a = 250$ au we find that decreasing $M_{*,\rm companion}$ from 0.2 to $0.1\,{\rm M}_{\odot}$ no longer results in fragmentation. A weaker $m = 2$ spiral mode is driven by the $0.1\,{\rm M}_{\odot}$ companion, which results in an increase in Σ and a decrease in Q at the spiral location, but the change is not significant enough to induce fragmentation. Instead, the spiral mode persists for two full binary orbits until the simulation ends. For the discs which do fragment, we again find a trend for discs to fragment earlier with increasing companion mass, finding $t_{\rm frag} = 3050$ and 1550 yr for $M_{*,\rm companion} = 0.2$ and $0.5\,{\rm M}_{\odot}$, respectively.

Considering the discs with $a = 325$ au we find that increasing $M_{*,\rm companion}$ from 0.2 to $0.5\,{\rm M}_{\odot}$ causes the disc to fragment, as the more massive star generates a stronger spiral mode. A single fragment forms after 4000 yr in the disc with $a = 325$ au and $M_{*,\rm companion} = 0.5\,{\rm M}_{\odot}$. Of all the discs simulated here, this is the widest periastron separation ($r_{\rm peri,actual} = 256$ au) for which we find fragmentation can be triggered.

None of the configurations where $a = 400$ au result in fragmentation, for any of the new companion star masses considered here.

4 DISCUSSION

4.1 Summary of results

We have identified a 'sweet spot' in the orbital parameter space of binary stars that may trigger fragmentation in a disc that does not fragment in isolation. We find that the disc-star interaction for intermediate separation binaries can be beneficial for fragmentation, with the exact range of ideal semimajor axes being a function of the orbital eccentricity, inclination, and companion star mass. A plot summarizing the companion's orbital parameters that are found to trigger fragmentation is included in Fig. 8, where we also highlight the minimum radius at which fragments formed in each disc.

In general, the companion will drive an $m = 2$ spiral through the disc, and fragmentation occurs at the inner region of one, or both, of the spirals as a result of the enhanced surface density pushing the disc over the fragmentation threshold. Heating of the disc induced by the companion is balanced by efficient cooling (see Fig. 3) and the instability is able to grow until fragmentation occurs.

We find that this is true for intermediate separation binaries with $150\,{\rm au} \leq a \leq 250\,{\rm au}$ ($116\,{\rm au} \leq r_{\rm peri,actual} \leq 186\,{\rm au}$), when considering circular binary orbits in the plane of the disc.

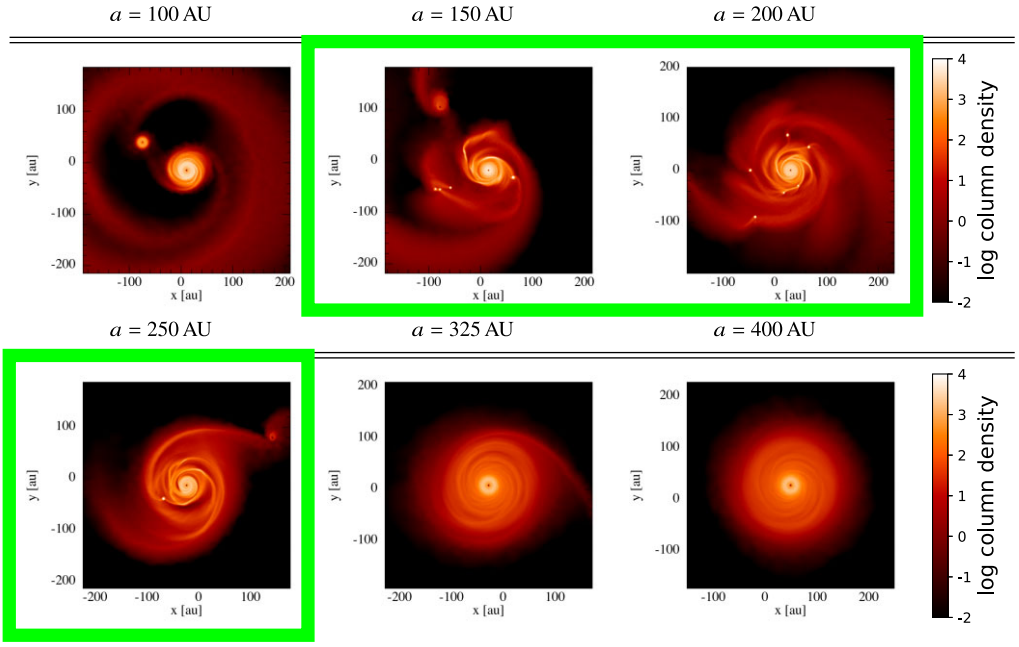

Figure 4. Final states of the discs where we keep the disc mass constant and consider small changes in the semimajor axis of the companion star. Disc set-up parameters are summarized in Table 3 and outlined in detail in Section 2.1.2. Green boxes are included to highlight disc configurations that resulted in fragmentation, when their reference run analogue did not.

For wide-orbit binaries the spiral induced by the companion becomes progressively weaker with increasing binary separation. When $a \gtrsim 400$ au and $M_{\rm disc} = 0.2\,{\rm M}_{\odot}$, the disc's final surface density profile and Q-profile are almost identical to the counterpart disc from the reference run with no companion.

Very short separation binary encounters, where the companion passes through the outer edge of the disc, become prohibitive to fragmentation. As the companion star passes through the disc, material is ejected and the remaining surface density profile is modified to be much steeper in the inner disc, and truncated at a distance slightly smaller than the distance of periastron passage. Hence, a much more compact and lower mass disc remains, and no fragmentation can occur.

When including an eccentricity in the binary orbit, we find a similar range in $r_{\rm peri,actual}$ capable of triggering fragmentation. From the suite considering non-circular orbits with moderate eccentricities ($e = 0.25$, 0.5) we find that semimajor axes $150\,{\rm au} \leq a \leq 400\,{\rm au}$ ($a \leq r_{\rm peri,actual} \leq 163$ au) can induce fragmentation. When considering highly eccentric orbits, with $e = 0.75$, none of our simulations fragment. This is generally because the high eccentricity causes the companion to pass through the disc at periastron passage.

When including an orbital inclination for the companion, we find its influence to become progressively lesser as we move its orbit away from the plane of the disc. When $i = 60^{\circ}$ we find the sweet spot in binary semimajor axis to be between $100\,{\rm au} \leq a \leq 200\,{\rm au}$ ($74\,{\rm au} \leq r_{\rm peri,actual} \leq 152$ au), which is reduced to being between $100\,{\rm au} \leq a \leq 150\,{\rm au}$ ($75\,{\rm au} \leq r_{\rm peri,actual} \leq 116$ au) when considering companions with $i = 90^{\circ}$. High inclination binary companions ($i = 60^{\circ}$, 90°) that pass through the disc outer edge are less destructive than when the binary orbit is in the plane of the disc, hence fragmentation can occur for slightly shorter separations when $i = 60^{\circ}$ and $i = 90^{\circ}$ compared to when $i = 0^{\circ}$.

The sweet spot found in binary separation is broadened as we increase the companion star's mass from 0.2 to $0.5\,{\rm M}_{\odot}$, as the higher mass companion drives a stronger spiral mode through the disc. We find companions with semimajor axes as wide as $a = 325$ au ($r_{\rm peri,actual} = 256$ au) can trigger fragmentation when $M_{*,\rm companion} = 0.5\,{\rm M}_{\odot}$. Equally, when considering less massive companions, the sweet spot in binary separation is narrowed. Only one of our simulations, with $a = 150$ au ($r_{\rm peri,actual} = 110$ au), results in fragmentation when $M_{*,\rm companion} = 0.1\,{\rm M}_{\odot}$. In the disc configurations that fragment for more than one value of $M_{*,\rm companion}$ (when $a = 150$ and 250 au), we find that the discs fragment faster with increasing companion mass.

4.2 Comparison to previous theoretical work

Previous work considering the possibility of fragmentation induced by the presence of a binary-star companion consists of three key papers in Nelson (2000), Mayer et al. (2005), and Boss (2006), with their results discussed in the review paper (Mayer, Boss & Nelson 2007a). Nelson (2000) and Mayer et al. (2005) found that the presence of a companion suppresses any instability due to significant tidal heating in spiral shock waves, thus stabilizing the disc. Boss (2006), however, concluded that binary companions may promote fragmentation, finding that spiral waves generated from the tidal interaction between the disc and the companion would typically go on to form dense, self-gravitating clumps. In Mayer et al. (2007a), the authors largely attribute the differences in their results to the use of an artificial viscosity in Nelson (2000) and Mayer et al. (2005), which is not included in Boss (2006), and would contribute significantly towards heating of the disc in the presence of a shock wave, given a sufficiently large artificial viscosity was included.

Various authors have also investigated the role of stellar flyby events in promoting or suppressing fragmentation in discs that would be marginally stable in isolation. The early work of Boffin et al. (1998) and Watkins et al. (1998a,b) found that, when considering isothermal discs, previously non-fragmenting discs would fragment

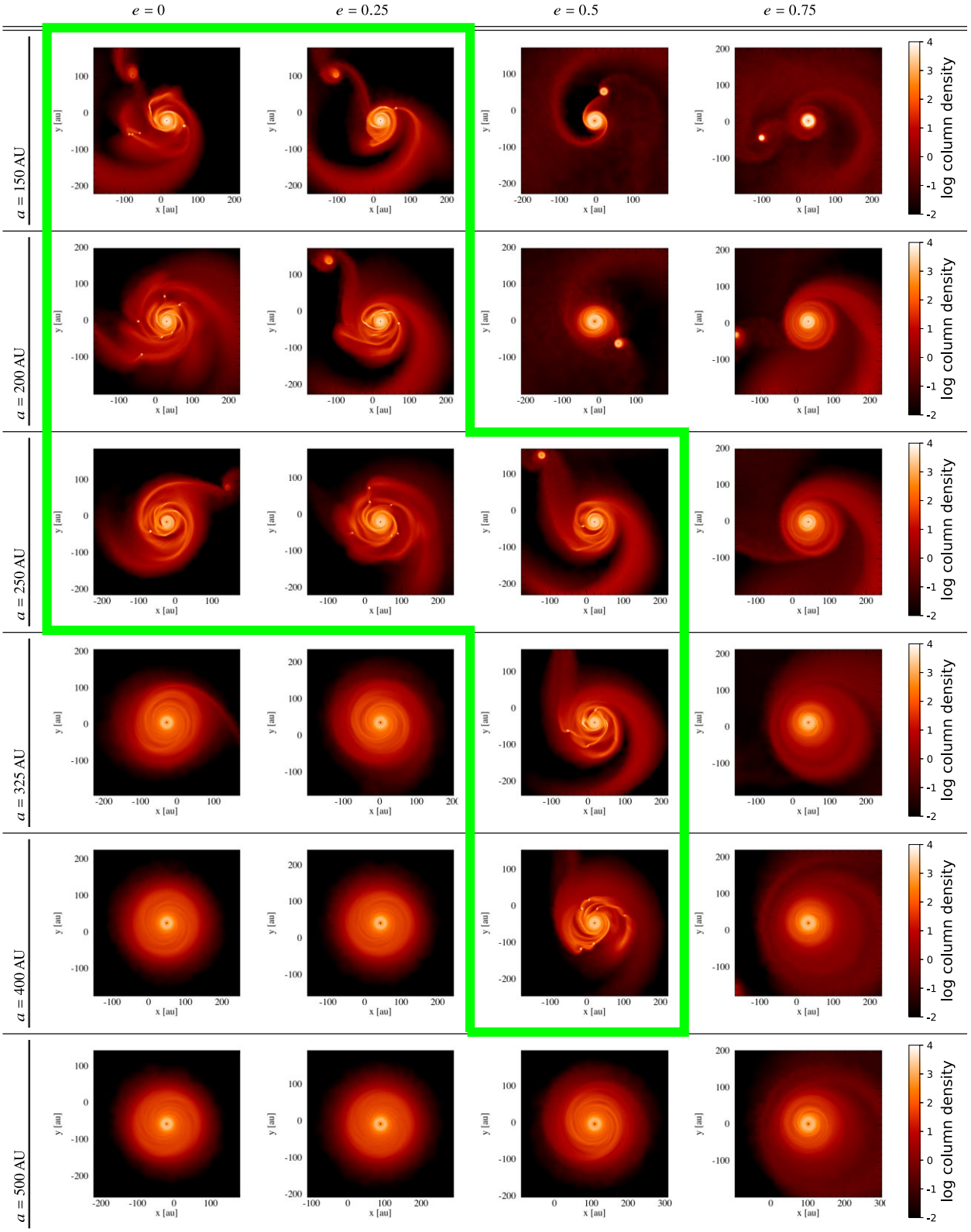

Figure 5. Final states of the discs where we vary the orbital eccentricity and the semimajor axis of the companion star. Disc set-up parameters are summarized in Table 4 and outlined in detail in Section 2.1.3. Green boxes are included to highlight disc configurations that resulted in fragmentation, when their reference run analogue did not.

during star–disc and disc–disc interactions. However, later models which included more realistic cooling found that heating of the disc during the stellar encounter was sufficient to stabilize it against fragmentation (Lodato et al. 2007; Forgan & Rice 2009).

Until now, most work has considered either simple cooling prescriptions, where the cooling time is proportional to the local orbital time (β-cooling, Gammie 2001; Rice et al. 2003), isothermal discs, or have not included an artificial viscosity that will capture

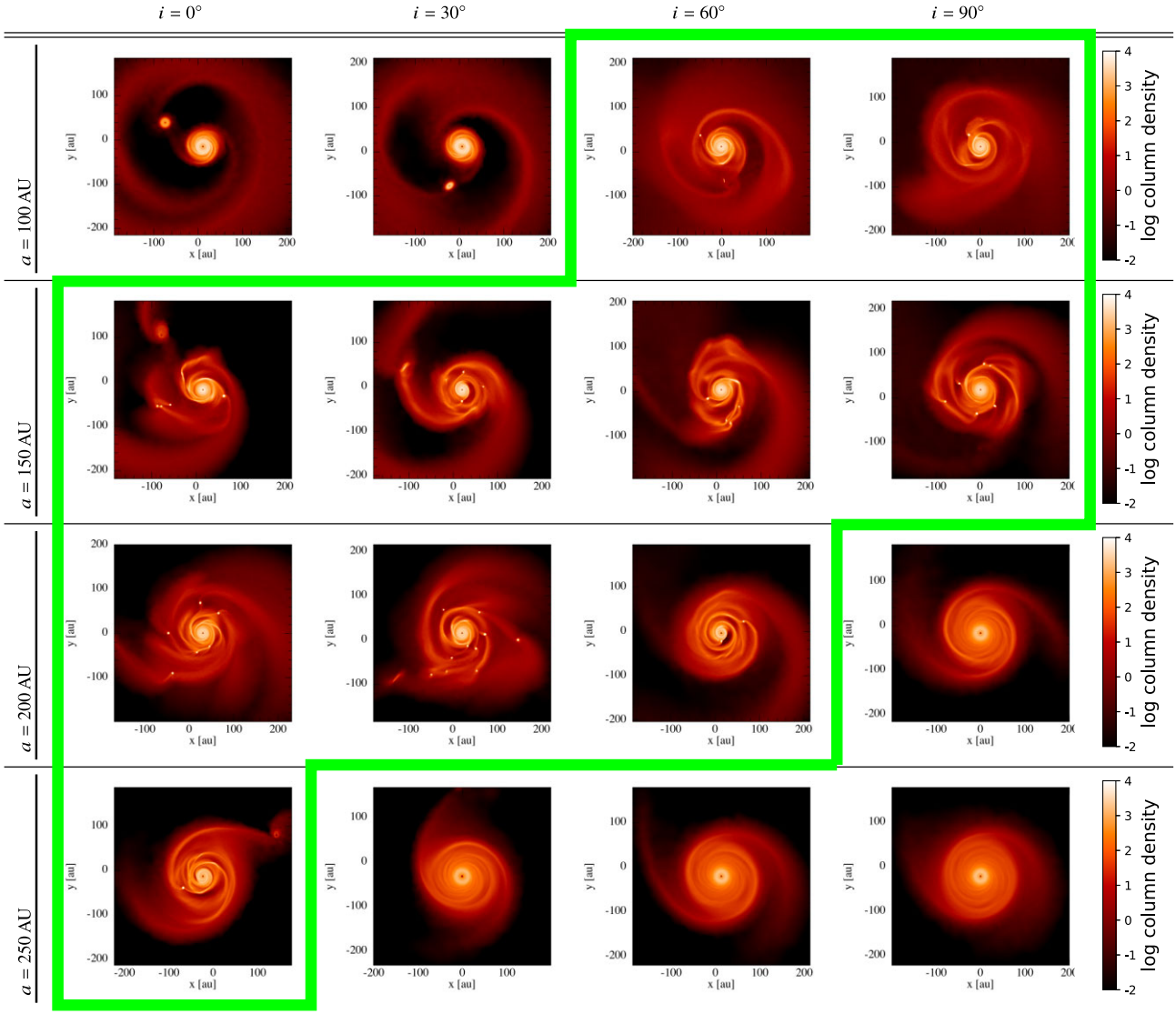

Figure 6. Final states of the discs where we vary the orbital inclination and the semimajor axis of the companion star. Disc set-up parameters are summarized in Table 5 and outlined in detail in Section 2.1.4. Green boxes are included to highlight disc configurations that resulted in fragmentation, when their reference run analogue did not.

heating from shocks. Including an algorithm to approximate radiation transport in our models (Forgan et al. 2009) allows us to model realistic disc cooling, hence we can realistically capture whether the disc is able to radiate away the additional energy generated through tidal heating during the binary encounter.

The aforementioned works generally also considered much more compact discs than we have modelled here (in the case of Nelson 2000; Mayer et al. 2005; Boss 2006; Lodato et al. 2007), or discs with $R_{\rm out} = 1000$ au (in the case of Boffin et al. 1998; Watkins et al. 1998a,b). However, owing to the simpler methods used to model disc cooling, their models are scale free and can be scaled to different physical units for comparison with the results here. Hence when comparing to the works of Boffin et al. (1998), Watkins et al. (1998a,b), Nelson (2000), Mayer et al. (2005), Boss (2006), and Lodato et al. (2007), we can use their ratios $r_{\rm peri}/r_{\rm out,disc}$ for direct comparison to our results. This is not the case for the results from Forgan & Rice (2009), who use the Forgan et al. (2009) hybrid radiative transfer method, and considered $R_{\rm out} = 40$ au discs. For the coplanar binary encounters considered here, we find that companions with $0.92 \leq r_{\rm peri}/r_{\rm out,disc} \leq 1.86$ trigger fragmentation. Only Lodato et al. (2007) considered binary encounters within this range, finding that no fragmentation occurred in their simulations.

Of the previous works, which include a similar cooling approximation as we use here, we find that our results broadly indicate the same thing. Forgan & Rice (2009) find that small separation, disc-penetrating encounters heat the disc material, while angular momentum transport and mass stripping result in a more stable disc configuration after the encounter. Large separation encounters have very little effect, becoming less significant as the periastron distance increases. However, intermediate separation encounters may modify the surface density profile of the disc, without causing significant heating, such that the disc is more unstable over a larger range of radii after the encounter. None of the discs in Forgan & Rice (2009) fragment, but the authors suggest that there could be some region of parameter space in periastron distance that may act to promote fragmentation.

Meru (2015), who used the flux-limited diffusion approximation (e.g. Mayer et al. 2007b), also found that further fragmentation may

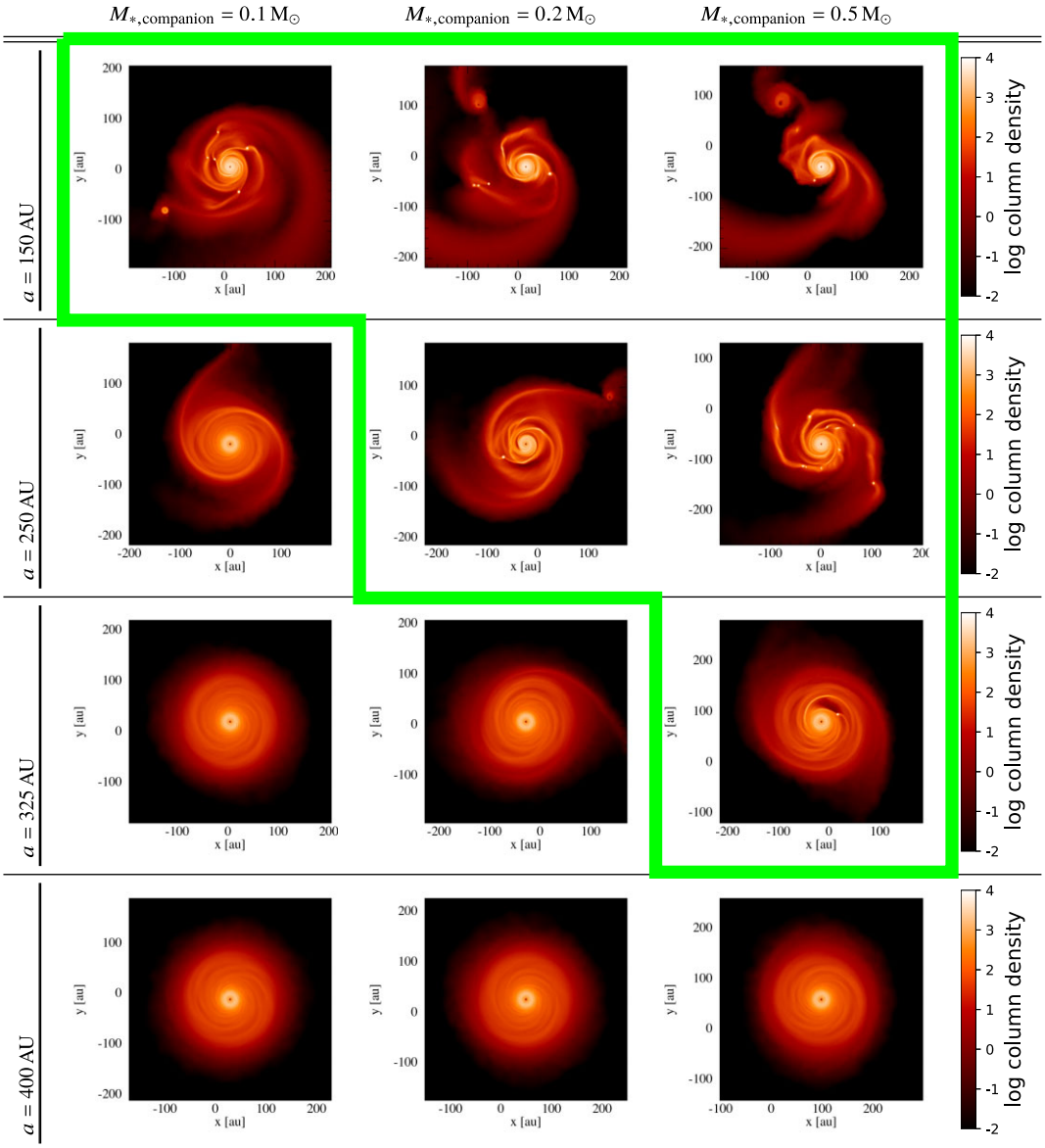

Figure 7. Final states of the discs where we vary the mass and the semimajor axis of the companion star. Disc set-up parameters are summarized in Table 6 and outlined in detail in Section 2.1.5. Green boxes are included to highlight disc configurations that resulted in fragmentation, when their reference run analogue did not.

be triggered in a disc that has fragmented already. The fragment that has initially formed causes material to be channelled inwards, increasing the density of the inner spirals, causing fragmentation.

Here, we have presented a suite of simulations that model realistic cooling using the Forgan & Rice (2009) radiative transfer approach. We find that efficient cooling is able to prevent the disc temperature from increasing significantly during the binary's periastron passage, and fragmentation can occur in the spiral regions of enhanced surface density that are driven by the companion.

4.3 Comparison to observations

Binaries are often neglected from observational and theoretical exoplanetary science, as they complicate the modelling of planet formation, as well as the detection and characterization of planetary systems. Most of the work (theoretical and observational) conducted so far on planets in binaries has focused on close-in binaries (separations of tens of au), generally agreeing that tight binaries (<50–100 au) hinder planet formation (Kraus et al. 2012, 2016; Bergfors et al. 2013; Kaib, Raymond & Duncan 2013). However, the first planets discovered in binary systems showed distinct orbital and physical properties from the rest of the planetary population, hinting at the possibility that binary companions could dramatically reorient the orbital configuration of planetary systems (Zucker & Mazeh 2002). Observations of binary-star systems suggest that stellar multiplicity at wider separations may play a key role in the formation of high-mass gas giant planets and brown dwarfs. Various surveys have found an excess of outer companions to stars with massive hot Jupiters or short-period stellar and substellar companions when compared to field stars, suggesting that binary-star systems on separations of a few hundred au may be favourable sites for the formation of these inner companions.

Beginning with their survey of solar-type spectroscopic binaries (SB), Tokovinin et al. (2006) found an excess of wide tertiary stellar

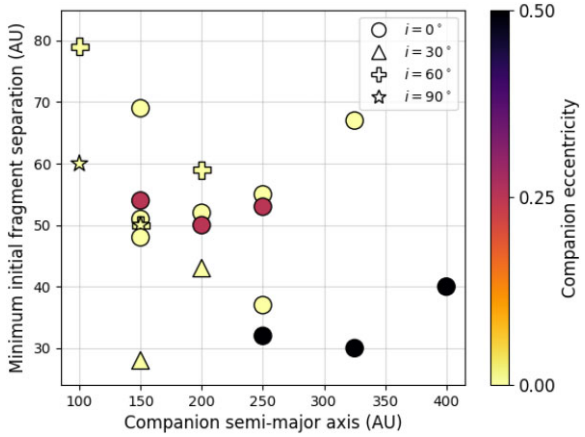

Figure 8. Summary of model parameters found to trigger fragmentation throughout this work, including the minimum radius at which fragments formed in each disc. A total of 20 systems presented here resulted in fragmentation. Companion orbital eccentricities are distinguished by different colours. Companion orbital inclinations are distinguished by different plot markers.

companions for SBs with periods from 1 to 30 d, rising to a frequency of 96 per cent for SBs with periods <3 d. In their series of 'Friends of hot Jupiters' papers, Ngo et al. (2016) searched for stellar companions to 77 systems hosting hot Jupiters. They found that 47 ± 7 per cent of stars hosting hot Jupiters have a binary companion with separations between 50 and 20 000 au (a value three times higher than found for field stars), although Moe & Kratter (2019) concluded that this excess was not significant after accounting for remaining statistical biases. None the less, Ngo et al. (2016) still observed a significant deficit of tight binary companions, with separations 50–100 au, compared to wider systems, consistent with the idea that shorter period binaries may be detrimental to planet formation (Wang et al. 2014; Kraus et al. 2016).

Using direct-imaging data, Fontanive et al. (2019) searched for wide-orbit binary companions to 38 stars known to host very massive hot Jupiters or brown dwarfs (7–60 M_{Jup}) on short periods (<1 au), finding a binary fraction close to 80 per cent for these systems on separations of 20–10 000 au, twice as high as for field stars, with a significance confirmed in Moe & Kratter (2019). Again, they observed a lack of binaries with separations of tens of au, and instead found an excess of intermediate separation binaries, with a peak in binary separation at ∼250 au. The binary frequency for massive giant exoplanets and brown dwarfs ($M > 7\,M_{Jup}$) was found to be higher than for lower mass hot Jupiters (0.2–4 M_{Jup}), suggesting that the stellar companion's influence may facilitate the formation of high-mass giant planets and brown dwarfs. The systems probed in Fontanive et al. (2019) also have a lower mean metallicity, consistent with that of the field (Moe et al. 2019), compared to hosts to genuine hot Jupiters like those studied in Ngo et al. (2016). Given the strong correlation seen between metallicity and the ability to form gas giant planets via CA (Mordasini et al. 2012; Jenkins et al. 2017), the high-mass inner substellar companions targeted in Fontanive et al. (2019) are therefore likely to have formed via GI rather than CA as for the lower mass hot Jupiters.

Recently, Fontanive & Bardalez Gagliuffi (2021) reached similar conclusions, finding that giant planets have a substantially larger raw stellar multiplicity fraction than sub-Jovian planets, and that this trend further increases up to a ∼30 per cent raw binary fraction for massive planet and brown dwarfs ($M > 7\,M_{Jup}$) on very short orbital separations (<0.5 au), with the most massive and shortest period substellar companions almost exclusively observed in multiple-star environments. These systems thus appear to follow the architectures of stellar SB, systematically observed as part of hierarchical triple systems (Tokovinin et al. 2006). Notably, Fontanive & Bardalez Gagliuffi (2021) showed that these extreme inner companions, with few analogues in (seemingly) single-star systems, were predominantly found to be in binaries with separations of few hundred au, and mostly on separations <250 au (despite a strong incompleteness at these separations) for substellar companions with masses above 7 M_{Jup}, consistent with results from Fontanive et al. (2019). In comparison, they found a peak around 600 au (subject to the same incompleteness biases) for binaries hosting lower mass planets or warm and cool gas giants on wider orbital separations, and these systems showed similar planet properties to the population of exoplanets orbiting single stars.

These results suggest that very wide binaries have no meaningful impact on the architectures of planetary systems, and confirm the idea that very tight binary systems have a negative impact on planet formation. In particular, it appears that binaries with tens to a few hundred au separations prevent planet formation for sub-Jovian and giant planets with masses up to a few M_{Jup}, while wider binaries can harbour such planets but without affecting their orbital properties. This indicates that the exoplanet population issued from CA only exists in binary configurations that are not disruptive to planet formation and do not influence the resulting planet properties. On the other hand, the higher mass population of giant planets and brown dwarfs on short-period orbits, likely formed via GI, is predominantly seen in intermediate separation binaries of few hundred au separations (Fontanive & Bardalez Gagliuffi 2021), which must thus play a role in their existence.

Here, we show with simulations of self-gravitating discs that such intermediate separation binary companions may assist in the formation of giant planets through means of the GI. We find that when introducing a stellar companion at a few hundred au into a disc configuration that would previously not fragment, fragmentation may be induced as the companion drives strong spirals that push the disc over the limit for instability. We find this to be true for binaries with semimajor axes between ∼100 and 400 au for the explored parameter space, with some dependence on binary orbital eccentricity, inclination, and companion mass. This is consistent with the binary projected separations observed by Fontanive et al. (2019) and Fontanive & Bardalez Gagliuffi (2021), a peak in the observed distribution at around 250 au. We also note that in our simulations the orbital properties of these intermediate separation binaries remain mostly unchanged after a full orbital period, as the companions do not pass directly through the disc; hence, the drag that they experience from the disc material is minimal.

Shorter period binaries and highly eccentric systems inhibit fragmentation as the disc–star interaction becomes destructive. As the companion passes through periastron, it will pass through the disc, leaving a compact, lower mass disc remaining. Hence, we would expect a lower frequency of GI-born planets within tight binary systems on separations of tens of au, which is also consistent with the shortfall of such systems in observations (Wang et al. 2014; Kraus et al. 2016; Ngo et al. 2016; Fontanive et al. 2019).

4.4 Outlook and implications for short-period, massive planets

Our work provides a viable formation pathway for the high-mass giant planets and brown dwarfs observed around components of multiple-star systems (Fontanive et al. 2019; Fontanive & Bardalez

Gagliuffi 2021). However, these substellar companions are actually observed on very short orbital periods (<1 au), much tighter than the typical formation locations from disc fragmentation.

In some cases, these objects could have been scattered by the binary stellar companion on to highly eccentric orbits and then been tidally circularized on to their current orbits (Rice et al. 2015). However, as discussed earlier, this is only possible for a subset of the systems presented in Fontanive et al. (2019).

Another possibility is that these objects may have naturally migrated to their current locations. Baruteau et al. (2011) showed that fragments forming in young, massive discs will undergo rapid, type I migration before having chance to open a gap, and may be able to reach the inner disc within a few orbital periods. However, it is uncertain as to what fraction of fragments will survive this migration, and what their eventual masses will be after tidal downsizing (Boley et al. 2010; Nayakshin 2010).

We also find indications that fragmentation triggered by the binary companion may be occurring closer in than is usually found for discs in isolation. In Fig. 3, considering the disc with an $a = 250$ au companion, the Q-profile reaches a minimum of $Q = 0.79$ at $R = 63$ au; hence, the first fragment initially forms at $R = 56$ au. In Fig. 8, we plot the minimum separation at which fragments form in each of our discs, including all systems with $M_{\rm disc} = 0.2\,{\rm M}_{\odot}$ that resulted in fragmentation. Of the 20 discs included in the plot, we find 9 systems produce fragments within $R = 50$ au, and 2 form fragments within $R = 30$ au.

It may then be that a combination of scattering, fragments forming close in, and rapid inward migration can produce the giant planets and brown dwarfs observed on very short orbital periods. While Baruteau et al. (2011) considered the subsequent migration of single fragments forming in a self-gravitating discs, it is not known how a binary companion or the formation of multiple fragments may affect this. We leave this question as subject of future work.

5 CONCLUSIONS

Observations of systems with close-in massive planetary and brown dwarf companions suggest that almost all host a binary stellar companion on a wider orbit (Fontanive et al. 2019). Also, the properties of the close-in objects are consistent with them having formed via fragmentation in a gravitationally unstable disc (Fontanive & Bardalez Gagliuffi 2021). However, disc fragmentation is only likely to operate in the outer parts of such discs, requiring that these objects somehow move from where they formed on to the close-in orbits they now occupy.

In some cases, the close-in object could have been scattered by the binary stellar companion and then undergone tidal circularization on to its current close-in orbit (Rice et al. 2015; Fontanive et al. 2019). However, in many cases, the tidal circularization time-scale is far too long for this to be a viable pathway for these systems. That such systems still typically host binary stellar companions suggests that these stellar companions still play a role in their formation.

To investigate this, we have conducted a series of 3D SPH simulations of self-gravitating discs with a binary stellar companion, exploring the companion's orbital parameter space for configurations that may trigger fragmentation in a marginally gravitationally unstable disc. We find a 'sweet spot' in which intermediate separation binaries can induce fragmentation, with the exact set of ideal orbital parameters being a function of the companion's semimajor axis, eccentricity, inclination, and mass.

Radiation transport is modelled using the Forgan et al. (2009) hybrid approach. For the discs modelled here, with outer radii $R_{\rm out} = 100$ au, we find that efficient cooling during intermediate separation ($100\,{\rm au} \lesssim a \lesssim 400\,{\rm au}$) binary encounters allows disc fragmentation to occur in a spiral region of enhanced surface density driven by the companion star. Short separation disc-penetrating ($a \lesssim 100$ au) encounters are generally destructive, as mass stripping and disc heating entirely wipe out any instability. This is also true of highly eccentric binary orbits, which result in the companion passing through the disc. However, highly inclined ($i \gtrsim 60^{\circ}$) disc-penetrating encounters can be less destructive, allowing shorter separation encounters to trigger fragmentation than when the binary orbit is in the plane of the disc. Wide-orbit binary encounters ($a \gtrsim 500$ au) have little effect on the disc properties, with the companion's influence becoming progressively lesser with increasing binary separation.

The range of binary separations found to promote fragmentation is consistent with the projected separations of the systems that display an excess of close-in giant planets and brown dwarfs (Wang et al. 2014; Kraus et al. 2016; Ngo et al. 2016; Fontanive et al. 2019; Fontanive & Bardalez Gagliuffi 2021). As our results show that intermediate separation binary systems could be favourable sites for the formation of massive substellar objects, we suggest that triggered fragmentation may contribute to the excess of massive planets and brown dwarfs observed around these systems. The question now remains how these fragments, initially formed on wide orbits, might have migrated to the very short separations (<1 au) where they are now currently observed, and will be the subject of future work.

ACKNOWLEDGEMENTS

The authors would like to thank the anonymous referee for their useful comments in helping to improve the work presented here. The simulations presented here were carried out using high-performance computing facilities funded by the Scottish Universities Physics Alliance (SUPA). 2D surface density plots were generated using SPLASH (Price 2007). CF acknowledges support from the Center for Space and Habitability (CSH). This work has been carried out within the framework of the NCCR PlanetS supported by the Swiss National Science Foundation. KR is grateful for support from the UK STFC via grant ST/V000594/1.

DATA AVAILABILITY

The model data generated in this study will be shared on request to the corresponding author.

REFERENCES

Baruteau C., Meru F., Paardekooper S.-J., 2011, MNRAS, 416, 1971
Benz W., 1990, in Buchler J. R., ed., Numerical Modelling of Nonlinear Stellar Pulsations Problems and Prospects. Kluwer Academic Publishers, Dordrecht, The Netherlands, p. 269
Bergfors C. et al., 2013, MNRAS, 428, 182
Boffin H. M. J., Watkins S. J., Bhattal A. S., Francis N., Whitworth A. P., 1998, MNRAS, 300, 1189
Boley A. C., 2009, ApJ, 695, L53
Boley A. C., Hayfield T., Mayer L., Durisen R. H., 2010, Icarus, 207, 509
Boss A. P., 1997, Science, 276, 1836
Boss A. P., 2000, ApJ, 536, L101
Boss A. P., 2006, ApJ, 641, 1148
Cadman J., Rice K., Hall C., Haworth T. J., Biller B., 2020a, MNRAS, 492, 5041
Cadman J., Hall C., Rice K., Harries T. J., Klaassen P. D., 2020b, MNRAS, 498, 4256
Cadman J., Rice K., Hall C., 2021, MNRAS, 504, 2877

Clarke C. J., 2009, MNRAS, 396, 1066
Dong R., Hall C., Rice K., Chiang E., 2015, ApJ, 812, L32
Durisen R. H., Boss A. P., Mayer L., Nelson A. F., Quinn T., Rice W. K. M., 2007, in Reipurth B., Jewitt D., Keil K., eds, Protostars and Planets V. University of Arizona Press, Tucson, p. 607
Fischer D. A., Valenti J., 2005, ApJ, 622, 1102
Fontanive C., Bardalez Gagliuffi D., 2021, Front. Astron. Space Sci., 8, 16
Fontanive C., Rice K., Bonavita M., Lopez E., Mužić K., Biller B., 2019, MNRAS, 485, 4967
Forgan D., Rice K., 2009, MNRAS, 400, 2022
Forgan D., Rice K., 2011, MNRAS, 417, 1928
Forgan D., Rice K., 2013, MNRAS, 432, 3168
Forgan D., Rice K., Stamatellos D., Whitworth A., 2009, MNRAS, 394, 882
Forgan D. H., Hall C., Meru F., Rice W. K. M., 2018, MNRAS, 474, 5036
Gammie C. F., 2001, ApJ, 553, 174
Hall C., Forgan D., Rice K., Harries T. J., Klaassen P. D., Biller B., 2016, MNRAS, 458, 306
Hall C., Forgan D., Rice K., 2017, MNRAS, 470, 2517
Hall C., Rice K., Dipierro G., Forgan D., Harries T., Alexander R., 2018, MNRAS, 477, 1004
Hall C. et al., 2020, ApJ, 904, 148
Haworth T. J., Cadman J., Meru F., Hall C., Albertini E., Forgan D., Rice K., Owen J. E., 2020, MNRAS, 494, 4130
Humphries J., Hall C., Haworth T. J., Nayakshin S., 2021, MNRAS, 502, 953
Jenkins J. S. et al., 2017, MNRAS, 466, 443
Johnson J. L., Li H., 2013, MNRAS, 431, 972
Kaib N. A., Raymond S. N., Duncan M., 2013, Nature, 493, 381
Kratter K. M., Murray-Clay R. A., Youdin A. N., 2010, ApJ, 710, 1375
Kraus A. L., Ireland M. J., Hillenbrand L. A., Martinache F., 2012, ApJ, 745, 19
Kraus A. L., Ireland M. J., Huber D., Mann A. W., Dupuy T. J., 2016, AJ, 152, 8
Laughlin G., Bodenheimer P., 1994, ApJ, 436, 335
Lin D. N. C., Pringle J. E., 1987, MNRAS, 225, 607
Lodato G., Rice W. K. M., 2004, MNRAS, 351, 630
Lodato G., Meru F., Clarke C. J., Rice W. K. M., 2007, MNRAS, 374, 590
Mayer L., Quinn T., Wadsley J., Stadel J., 2002, Science, 298, 1756
Mayer L., Wadsley J., Quinn T., Stadel J., 2005, MNRAS, 363, 641
Mayer L., Boss A., Nelson A. F., 2007a, preprint (arXiv:0705.3182)
Mayer L., Lufkin G., Quinn T., Wadsley J., 2007b, ApJ, 661, L77
Meru F., 2015, MNRAS, 454, 2529
Meru F., Bate M. R., 2010, MNRAS, 406, 2279
Meru F., Juhász A., Ilee J. D., Clarke C. J., Rosotti G. P., Booth R. A., 2017, ApJ, 839, L24
Moe M., Kratter K. M., 2019, preprint (arXiv:1912.01699)
Moe M., Kratter K. M., Badenes C., 2019, ApJ, 875, 61
Monaghan J. J., 1992, ARA&A, 30, 543
Mordasini C., Alibert Y., Benz W., Klahr H., Henning T., 2012, A&A, 541, A97
Nayakshin S., 2010, MNRAS, 408, L36
Nayakshin S., Fletcher M., 2015, MNRAS, 452, 1654
Nelson A. F., 2000, ApJ, 537, L65
Nero D., Bjorkman J. E., 2009, ApJ, 702, L163
Ngo H. et al., 2016, ApJ, 827, 8
Nielsen E. L. et al., 2019, AJ, 158, 13
Paczynski B., 1978, Acta Astron., 28, 91
Paneque-Carreño T. et al., 2021, ApJ, 914, 88
Pérez L. M. et al., 2016, Science, 353, 1519
Pollack J. B., Hubickyj O., Bodenheimer P., Lissauer J. J., Podolak M., Greenzweig Y., 1996, Icarus, 124, 62
Price D. J., 2007, Publ. Astron. Soc. Aust., 24, 159
Price D. J. et al., 2018, Publ. Astron. Soc. Aust., 35, e031
Rafikov R. R., 2005, ApJ, 621, L69
Rice W. K. M., Armitage P. J., 2009, MNRAS, 396, 2228
Rice W. K. M., Armitage P. J., Bate M. R., Bonnell I. A., 2003, MNRAS, 339, 1025
Rice W. K. M., Mayo J. H., Armitage P. J., 2010, MNRAS, 402, 1740
Rice K., Lopez E., Forgan D., Biller B., 2015, MNRAS, 454, 1940
Rodríguez L. F., Loinard L., D'Alessio P., Wilner D. J., Ho P. T. P., 2005, ApJ, 621, L133
Santos N. C., Israelian G., Mayor M., 2004, A&A, 415, 1153
Schlaufman K. C., 2018, ApJ, 853, 37
Stamatellos D., Whitworth A. P., 2009, MNRAS, 392, 413
Stamatellos D., Whitworth A. P., Bisbas T., Goodwin S., 2007, A&A, 475, 37
Tobin J. J., Hartmann L., Chiang H.-F., Wilner D. J., Looney L. W., Loinard L., Calvet N., D'Alessio P., 2012, Nature, 492, 83
Tobin J. J. et al., 2015, ApJ, 805, 125
Tokovinin A., Thomas S., Sterzik M., Udry S., 2006, A&A, 450, 681
Toomre A., 1964, ApJ, 139, 1217
Veronesi B., Paneque-Carreño T., Lodato G., Testi L., Pérez L. M., Bertin G., Hall C., 2021, ApJ, 914, L27
Vigan A. et al., 2017, A&A, 603, A3
Vigan A. et al., 2021, A&A, 651, A72
Vorobyov E. I., Basu S., 2010, ApJ, 714, L133
Wang J., Xie J.-W., Barclay T., Fischer D. A., 2014, ApJ, 783, 4
Watkins S. J., Bhattal A. S., Boffin H. M. J., Francis N., Whitworth A. P., 1998a, MNRAS, 300, 1205
Watkins S. J., Bhattal A. S., Boffin H. M. J., Francis N., Whitworth A. P., 1998b, MNRAS, 300, 1214
Zucker S., Mazeh T., 2002, ApJ, 568, L113

This paper has been typeset from a TEX/LATEX file prepared by the author.